Modeling the Effects of Crevice Former, Particulates, and the Evolving Surface Profile in Crevice Corrosion

A. S. Agarwal[a], U. Landau[a], Xi Shan[b] and J. H. Payer[b]

[a] Department of Chemical Engineering
[b] Department of Material Science and Engineering
Case Western Reserve University, Cleveland Ohio 44106 USA

Crevice corrosion may initiate in confined regions due to transport limitations, followed by an accumulation of a highly corrosive chemistry, capable of dissolving the metal. The metal and the crevice former surface roughness, the presence of particulates under the crevice former and the accumulation of solid corrosion products at the corroding site would significantly affect the current and potential distribution at the anode by increasing the ohmic potential drop. Most crevice corrosion models focus on a smooth walled crevice of uniform gap and do not account for the changing profile after crevice corrosion has been initiated. In this work we analyze the crevice (anodic) region and apply current and potential distribution models to examine the effects of the perturbed surface topography. The analysis focuses on three related issues: (i) the effects of surface roughness of the metal and the crevice former, (ii) the effects of particulates under the crevice former, and (iii) the evolution of the crevice profile with corrosion product accumulation at the active, anodic region.

Introduction

Crevice corrosion is a mode of localized corrosion which is particularly critical to the long-term performance of corrosion resistant alloys in high-temperature aqueous environments. In a geometrically confined region such as a crevice, formed by two metal or metal-insulator surfaces in close proximity to one another, transport limitations readily lead to the depletion of oxygen. Metal ions hydrolyze, and chloride ions migrate into the crevice to maintain electroneutrality. An aggressive crevice solution chemistry with a low pH and a high [Cl^-] is thus formed (1 - 4). When sufficiently aggressive, a so-called 'critical solution chemistry' develops within the crevice which is capable of breaking down the passive film. The propagation of crevice corrosion from this point onwards significantly depends on the potential distribution inside the crevice.

As shown in Figure 1, a critical solution is generated at a critical distance (X) within the crevice. This critical distance depends on the corrosion resistance of the metal/alloy composition, the tightness of the crevice former, and also on the bulk solution chemistry (4, 5). Concentration and potential gradients along the critical distance are indicated by the family of polarization curves, as shown in Figure 1. In such a crevice corrosion system the majority of the anodic current is produced by the corroding site, while the metal/alloy along the critical distance can be assumed to be under passive dissolution kinetics. Physical irregularities along this critical distance such as constrictions resulting from surface roughness at the metal-crevice former contact and the presence of inert

particles under the crevice former would lead to an increased ohmic resistance to the current. Accumulation of corrosion products at the corroding site would alter the shape and propagation rate of the crevice corrosion site. While such features are commonly encountered in actual crevices, there has been limited analysis of the effects of these physical features on the rate and propagation of crevice corrosion (5). The purpose of this work has been to develop modeling techniques to account for these effects within the framework of the traditionally used crevice corrosion models.

Objectives

The specific objective of this work has been to analyze the ohmic (voltage drop or 'IR') effects resulting from the above stated physical/geometrical features encountered in real crevices, and apply suitable models to characterize the intricate crevice geometry in terms of a simpler homogeneous model, which is traditionally used to represent crevice corrosion systems. The following three issues were specifically addressed: (i) the effects due to surface roughness of the metal and the crevice former, (ii) the effects of particulates under the crevice former, and (iii) the evolution of the crevice profile with corrosion product accumulation at the active, anodic region. Although only ohmic limitations were considered in the present work, we intend to account for the effects of changes in solution chemistry in the near future.

Effect of Crevice-Former Surface Irregularities and Metal Roughness

In real or experimental crevice corrosion systems, the crevice former and the metal substrate typically have surface roughness of the order of or greater than the nominal crevice gap [as indicated by G_a in Figure 2 (a)]. The narrow gap along the rough surface creates constriction to the current, as shown schematically in Figure 2 (a). This is particularly the case for highly corrosion resistant alloys such as Alloy C-22. Crevice corrosion experiments with C-22 indicated that corrosion occurs only when the crevice former is pressed tightly against the metal surface, leaving a crevice gap of sub-micron scale (8). These cross sectional variations will cause a particularly large increase in the ohmic resistance to the current at regions of narrow constrictions (Figure 2 (a)). Our goal was to develop a methodology for representing a crevice with surface roughness in terms of an equivalent 'idealized' smooth walled crevice as shown in Figure 2 (b).

Constriction Factor Analysis: The extent of resistance offered by the surface roughness depends on the shape and size of the constrictions. We follow a procedure outlined by Lanzi and Landau for modeling porous electrodes (9). In this analysis, the cross sectional variations of the crevice system can be represented in terms of a constriction factor τ and a porosity ε which depend on the geometry of the rough interface. These parameters can then be applied to define an equivalent crevice system with smooth walls, representing the original crevice. A crevice former with rectangular cross sectional variations is shown in Figure 3. Such a system can be represented by several equal repetitive units, each of length λ. The parameter ξ is used to define the extent of constriction. The maximal gap is indicated by 'h' and the height of the constriction is represented as 'ξh'. The mean cross sectional area <S> is calculated based on the geometry. This parameter is then used to obtain the constriction factor 'τ' (using Eq. [1]) and the porosity 'ε' (using Eq. [2]). The details of this calculation are provided in Ref. (9).

$$\tau = \langle S \rangle * \langle 1/S \rangle = (1+\xi)(1-\xi+\xi^2) \quad [1]$$

$$\varepsilon = \langle S \rangle / \lambda^2 = (1-\xi^2) \quad [2]$$

Using these parameters, the average potential drop along a unit length 'λ' for a constant axial current I' can be expressed in terms of the ohm's law:

$$\frac{\phi(z+\lambda)-\phi(z)}{I'} = \frac{\langle\phi\rangle(z+\lambda)-\langle\phi\rangle(z)}{I'} = \left[-\frac{\lambda\tau}{\kappa W G_a \varepsilon}\right] = \left[-\frac{\lambda}{\kappa W G'_a}\right] \quad [3]$$

κ is the conductivity of the electrolyte within the crevice and W is its width. The expression within the brackets on the right-most side in Eq. [7] represents the resistance of a smooth cross-sectional channel with a gap G'_a. Accordingly, the gap (G_a) for the non-uniform system then can be represented in terms of an equivalent smooth wall gap (G'_a) that is a function of constriction factor and the porosity.

$$G'_a = G_a \times \frac{\varepsilon}{\tau} \quad [4]$$

The above analysis can be applied to any crevice system provided that its geometry is known.

Computational Verification: The potential distribution in a crevice former with the same geometry as evaluated above was numerically modeled in order to test the constriction factor analysis. The value of the constriction parameter ξ was varied from 0.3 to 0.9 and the corresponding crevice gap G_a' was obtained in terms of τ and ε. A commercial simulation software, FEMLAB® (6) was used to compute the results. A constant current anode was modeled at one end of the crevice system of known length, representing the active corroding site under the crevice former (Figure 3). A virtual cathode ("primary" electrode with infinitely fast kinetics at 0 V_{NHE}) was placed at the other end of the crevice system, representing the crevice mouth. This cathode is the sink for the entire anodic current produced inside the crevice. The crevice gap (G_a), its length (L) and total anodic current were varied, and the potential drop across the crevice was computed and compared for the two systems, viz. the crevice system with varying cross sectional area and the equivalent smooth walled system based on the constriction factor analysis.

Results and Discussion: The schematic in Figure 3 shows the geometry of the crevice former. For this geometry, the effect of the constriction parameter (ξ) on the equivalent crevice gap (G_a') is shown in Table I. It is evident that an increase in the size of the constriction (ξ increasing from 0.3 to 0.9) provides a greater resistance to the current and hence the modified crevice gap needs to be further reduced (G_a'/G_a decreases from 0.95 to 0.42). Figure 4 shows the comparison between simulation results and analytical modeling of constriction effects due to non-uniform crevice former. As noted, the constriction factor analysis is within 5 to 15 % of the numerical simulations. A few other complex geometries with constrictions on both the crevice former and the underlying metal were also evaluated and the results were within 10 – 15%. Thus, the constriction factor analysis adequately predicts the constriction effects due to a crevice former with a

rough surface. Such an analysis is useful for analyzing complex geometries of crevice systems in terms of equivalent smooth-walled homogeneous systems. These simpler equivalent systems would more amenable to the modeling of other phenomena associated with crevice corrosion.

Table I: Ratio of equivalent 'smooth' crevice gap (G_a') to the maximum gap of a non-uniform crevice former (G_a) as a function of the extent of constriction (ξ) – Analytical Computations.

ξ	porosity (ε)	tortuosity (τ)	G_a'/G_a
0	1	1	1.00
0.3	0.96	1.01	0.95
0.5	0.88	1.04	0.84
0.7	0.76	1.14	0.66
0.9	0.60	1.43	0.42

Effect of Particles Present under the Crevice Former

Crevice corrosion could occur under non-submerged conditions, i.e. in the presence of moist layers of dust, particulates, and deposits. Such systems could have particulates under the crevice former (Figure 5). These could be deposited as dust before the initiation of the corrosion or accumulate as solid insoluble products or deposits produced by earlier corrosion events. Presence of particulates under the crevice former would lead to an additional resistance to the flow of current due to a high localized IR drop. If the blocking effect of particles inside the narrow crevice on the potential distribution can be accounted for quantitatively by modifying the conductivity of the electrolyte, the crevice corrosion system would be reduced to a much simpler equivalent system with a modified conductivity and no particles. The rationale for the modeling presented in this section is to apply and test such a correction for the effect of particulates and obtain a simpler equivalent crevice model. Such a modified crevice model would be much more amenable for use in complex full scale modeling of ion-ion interactions, precipitation etc. inside the crevice.

Accounting for Particles in terms of an Effective Electrolyte Conductivity (κ_{eff}): The presence of particles in the electrolyte along the critical distance between the crevice mouth and the actively corroding site would increase the resistance by blocking the volume of the electrolyte which otherwise would have been available for the current. Based on our earlier work of modeling cathode currents in presence of particulates (10), a suitable correction for accounting for this volume blockage effect can be made on the basis of Bruggeman's equation for the equivalent conductivity (11). For a uniform distribution of particulates in the electrolyte, Bruggeman's equation, [5], can be used to obtain an effective conductivity, κ_{eff}, once the volume fraction occupied by the particles ($\Phi_{particles}$) is known.

$$\kappa_{\text{eff}} = \kappa_{bulk}(1-\phi_{particles})^{\frac{3}{2}} \qquad [5]$$

Figure 6 illustrates the dependence of the effective conductivity on the volume fraction. At high volume coverage (80% and above), the effective conductivity is reduced by an order or magnitude or more, thus, significantly increasing the ohmic potential drop. This would considerably affect the dissolution rate of the crevice.

Computational Modeling Methodology: To verify the validity of Eq. [5] accounting for the resistance of a particle layer, we compare the results provided by this equation to numerical simulations, using FEMLAB® (6). Uniform distributions of a single layer of particles in the region between the crevice mouth and the corroding site were analyzed. The size, shape, and volume fractions of the particles were varied. Based on the volume fraction of the particles, κ_{eff} was calculated and an equivalent system with no particles but with κ_{eff} as the solution conductivity (instead of κ_{bulk}) was simulated. The total current flowing along the crevice for a constant potential drop was simulated and compared for both systems. The range of conductivities evaluated was 0.001 to 1 S/cm. The crevice gap was varied between 1 and 100 μm, and the crevice lengths used were 10 to 100 times the crevice gap.

Results and Discussion: Figure 7 shows the simulation results with particles and in an equivalent system without particles, employing, however, an equivalent effective conductivity. In Figure 7 (a), spherical particles were considered under the crevice former. The results indicate the value of the total current produced for applied potential across the crevice. The length of the crevice is 100 μm and the crevice gap, G_a, is 10 μm. The solution conductivity is 0.1 S/cm. The simulations with no particles present show, as expected, a significantly higher current than that with particles. In the results labeled 'Bruggeman's correction', the conductivity of the electrolyte was adjusted to κ_{eff} based on the volume fraction of the spherical particles ($\Phi_{particles}$ = 52%) using Eq. [5]. It is observed that the equivalent homogeneous system (no particles) with the adjusted conductivity closely predicts the simulation results of the 'actual' system with particulates. Similar results were observed for cubical particles as shown in Figure 7 (b). The simulations were repeated by changing the bulk solution conductivity, length of crevice, crevice gap, the volume fraction and shape of particles. In all cases, applying an effective conductivity in a homogeneous (no particulate) system accounted for the presence of particles. Thus, if the volume fraction of the particles under the crevice former is known, the complex system with particles can be reduced to an equivalent homogeneous system by applying Bruggeman's correction.

Effect of Corrosion Product Accumulation on the Damage Profile Evolution

In crevice corrosion tests conducted on alloy C-22 in 4 M NaCl at 100 °C, solid corrosion products were observed at the corroding site (8). EDS analysis of the corrosion products indicate that these consist of inert solid oxides of Mo, W and Cr. The Pourbaix diagrams of Mo and W show that oxides of these species are likely to exist as insoluble products, even under the low pH conditions required for the formation of the critical crevice chemistry for Alloy C-22 (12). The corrosion products appear to be fine particulates tightly packed under the crevice former but loosely attached to the underlying alloy surface (Figure 8). Among the likely effects of the accumulation of solid oxides at the corroding site is the increase of ohmic resistance in the corroding region and the alteration of the damage evolution profile. In this section, the evolving profile of the corroding crevice with particulate accumulation at the corroding site was simulated. The effect of the deposit was accounted in terms of a decrease in the effective local solution conductivity at the corroding site, based on the volume fraction of the inert solid particles accumulated as a function of time. This damage profile was compared to the case where no solid corrosion products are present.

Effect of Corrosion Products: Similar to the effect of particulates under the crevice former, the formation of solid oxides at the corroding site and its accumulation with time increases the ohmic resistance. It is assumed that 50% of the corroded metal forms insoluble inert metal oxide particles. Although, the actual fraction of the corrosion products might vary, the trend in damage profile propagation still remains. The density of the corrosion products was assumed to be half that of the metal, close to the actual densities of oxides of Mo, W and Cr and Alloy C-22. Hence, the volume of the solid product is about equal to the volume of the corroded metal. It was also assumed that the particles are uniformly distributed in the solution within the corroding pit. Based on these assumptions, the effective solution conductivity within the pit was calculated using Bruggeman's Equation, [5].

Computational Modeling of the Moving Boundary Problem: The modeled crevice corrosion system is shown in Figure 9 (a). The crevice gap, G_a, was held at 1 μm. The active corroding site was placed at a distance of 100 μm from the crevice mouth. The metal surface along the crevice length (100 μm) was assumed to be passive, i.e., act as an insulator. The initial length of the actively corroding anode site was 10 μm. This signifies that the critical chemistry is formed at a distance of 100 μm within the crevice, over a length of 10 μm. Anode kinetics for the dissolution of a Ni-Cr-3Mo alloy at pH = 1 and at room temperature was applied to the corroding site and kept constant at all times (13). This alloy composition is quite similar to that of Alloy C-22 and the experimental conditions of the anodic polarization are similar to those that persist for the critical crevice solution chemistry for Alloy C-22 (12). The crevice mouth was held at 0.05 V_{NHE}, which is close to the repassivation potential (E_{rp}) of Alloy C-22 (13). The methodology for the application of the boundary conditions (potential/kinetics at the electrodes) was similar to that used earlier for the modeling of the cathode region (10). The average atomic weight of the corroding metal was taken as 58.5 and it was assumed that all the current generated at the anode led to metal dissolution (100% current efficiency). Laplace's equation for the potential, Φ, is solved in the solution (Eq. [6]) to obtain the potential and current distribution at the anode site.

$$\nabla^2 \Phi = 0 \qquad [6]$$

Cell-Design software (7) was used to solve the moving boundary problem applying a progression of time steps. The software determines the volume of the dissolving region based on Faraday's law for a given time-step and thus a corroded geometry of the surface is generated at the end of each time step. Based on the assumptions made for the solid oxide formation at the anode site discussed in the previous section, a new effective conductivity was calculated using Bruggeman's equation, [5], and the simulation was re-run for another time step. A schematic of a corroded crevice with particulates is shown in Figure 9 (b). The time steps were kept small (~0.1 to 0.3 min) to minimize computational inaccuracies and to better represent the unsteady-state problem through the finite time steps.

Results and Discussion: Figure 10 shows the results for the moving boundary simulations performed on the crevice corrosion system shown in Figure 9. Initially, the current density over the anode is quite uniform (Figure 10 (b)). As corrosion proceeds, the volume fraction of the corrosion products occupying the corroding site increases, leading

to a decrease in the effective conductivity (Figure 10 (c)). This causes a decrease in the current density along the anode. The symmetrical propagation of the corroding site is observed as uniform cylindrical evolution of damage in Figure 10 (a). At later time steps, the propagation of the corroding site shifts to a non-uniform tear-shaped evolution which advances towards the crevice mouth. This process becomes pronounced when the volume fraction of the particles exceeds about 80% leading to an effective conductivity decrease by more than an order of magnitude ($\kappa_{eff}/\kappa_{bulk} < 0.1$). This propagation of corrosion damage towards the crevice mouth was substantiated by examining the current density profiles along the anode. These indicate a higher rate of corrosion towards the crevice mouth as compared to the trailing end.

For comparison, simulations were also run for a corroding crevice, assuming that there was no accumulation of solid corrosion products. In this case, the effective conductivity at the corroding site was kept constant at a value equal to the bulk conductivity ($\kappa_{eff} = \kappa_{bulk} = 0.1$ S/cm) for all time steps. The results depicted in Figure 11 (a) indicate a symmetrical, cylinder-like propagation of the corroding site, with no appreciable shift towards the crevice mouth, as noted for the case with particulates (Figure 11 (b)). This was corroborated by the uniform current density curves observed for the 'no-particulate' case as shown in Figure 11 (c). These results indicate that the formation and accumulation of solid products at the corroding site are expected to lead to a tear-shaped damage evolution profile, propagating towards the crevice mouth.

Conclusions

The effect of surface roughness, presence of particles under the crevice former, and corrosion product accumulation on the current distribution in the anodic region of a corroding crevice was modeled. Applying the constriction factor model, the surface roughness present in crevices, which is likely to cause a high localized IR drop, is accounted for by a smooth-walled crevice system with an equivalent crevice gap. The presence of particles under the crevice former was seen to increase the ohmic potential drop and decrease the anodic current. This particulate effect can be represented in terms of an equivalent homogeneous system with modified electrolyte conductivity using Bruggeman's equation. This approach provides a means for representing a complex crevice with surface roughness and particulates in terms of an equivalent homogeneous system. Such a simpler equivalent system would be more amenable for modeling of other complex phenomena in crevice corrosion. Simulation of a crevice with solid oxide accumulation at the corroding site indicated a non-symmetrical tear-shaped evolution of the corroding site which preferentially grows towards the crevice mouth.

Acknowledgments

Support by the Science & Technology Program of the Office of the Chief Scientist (OCS), Office of Civilian Radioactive Waste Management (OCRWM), U.S. Department of Energy (DOE), is gratefully acknowledged. The work was performed under the Corrosion and Materials Performance Cooperative, DOE Cooperative Agreement Number: DE-FC28-04RW12252. The views, opinions, findings, and conclusions or recommendations of authors expressed herein do not necessarily state or reflect those of the DOE/OCRWM/OCS.

References

1. J. W. Oldfield and M. H. Sutton, *Br. Corros. J.,* **13,** 1 (1978).
2. M. G. Fontana, *Corrosion Engineering*, 3rd Edition, p.53, McGraw Hill, New York (1985).
3. H. W. Pickering, *Corrosion,* **42,** 125 (1986).
4. P.O. Gartland, in *Proceedings of Corrosion/96 Research Topical Symposia*, p. 311, NACE International, Houston, TX (1996).
5. M. K. Watson and J. Postlethwaite, *Corrosion Science,* **32,** 1253 (1991).
6. "FEMLAB", multi-physics modeling package, COMSOL Ltd., Burlington, MA USA.
7. "Cell-Design", computer aided design software for electrochemical cells, L-Chem, Inc., Shaker-Heights, OH USA.
8. X. Shan and J. H. Payer, *ECS Trans.,* **3,** Oct. (2006) *(to be published).*
9. O. Lanzi, and U. Landau, *J. Electrochem. Soc.,* **137,** 585 (1990)
10. A. S. Agarwal, U. Landau, Xi Shan and J. Payer, *ECS Tran.,* **1,** (16) 67 (2006).
11. D. A. G. Bruggeman, *Ann. Phys. Leipzig,* **24,** 636 (1935).
12. Z. Y. Chen, F. Cui and R. G. Kelly, *ECS Trans.,* **3,** Oct. (2006) *(to be published).*
13. F. J. Presuel-Moreno, F. Bocher, J. Scully and R. G. Kelly, *ECS Trans.,* **3,** Oct. (2006) *(to be published).*

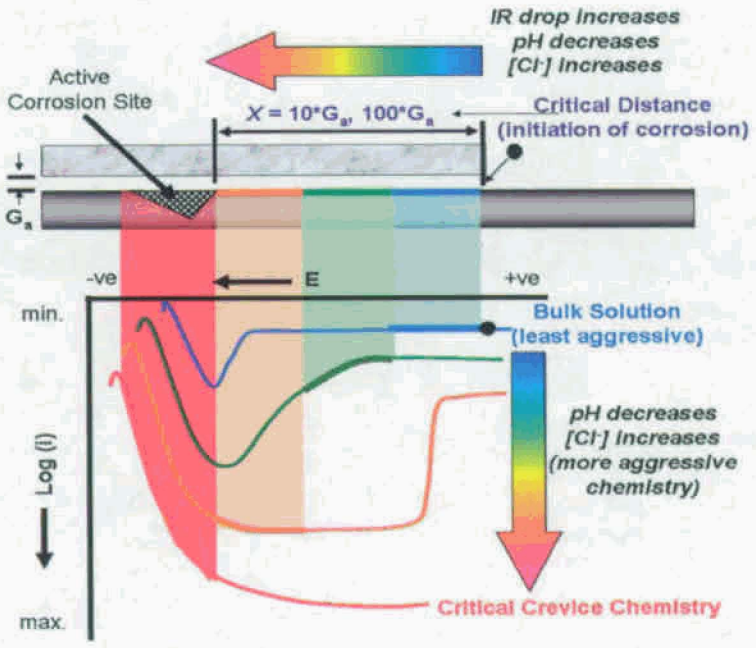

Figure 1: Schematic diagram of the crevice corrosion system depicting the anodic polarization curves as a function of the solution chemistry. The critical distance within the passive crevice region which is required for the formation of the critical chemistry is indicated.

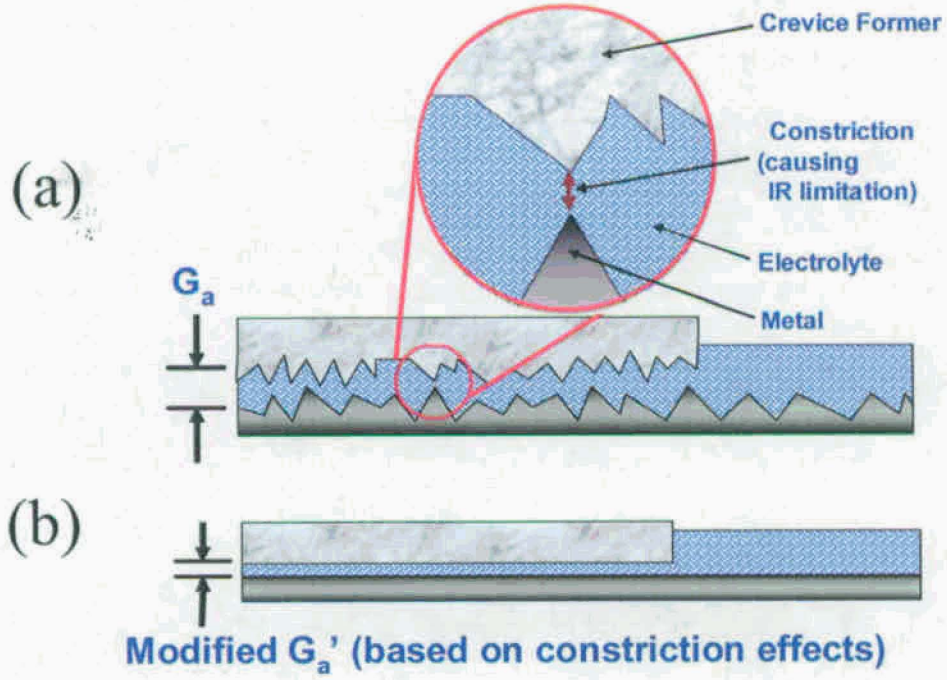

Figure 2: (a) Constrictions in real or experimental crevices associated with surface roughness. (b) Equivalent 'idealized' system with smooth walls and an equivalent crevice gap (G_a').

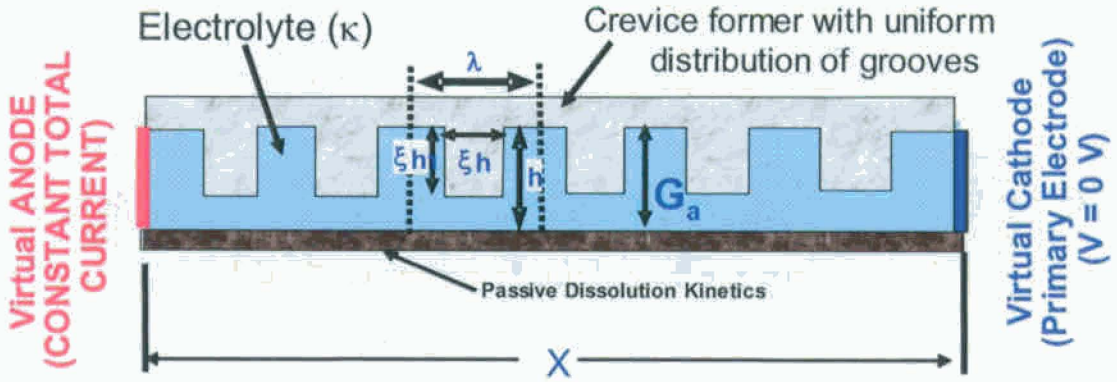

Figure 3: A crevice former geometry with cross-sectional rectangular roughness elements modeled using the constriction factor analysis 'Decoupled Anode Model'.

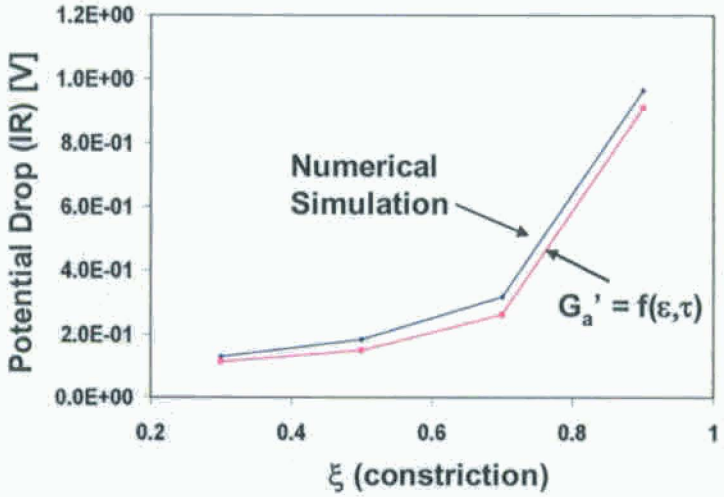

Figure 4: Potential drop as a function of constriction (ξ). The numerical simulation for the geometry shown in Figure 3 is compared to the equivalent system evaluated using the constriction factor analysis ($G_a' = f(\varepsilon,\tau)$). Experimental parameters: I_{total} (anode) = 1 mA, G_a = 10 μm, X = 100 μm, κ = 0.1 S/cm (~ 1 M [Cl^-]). % Difference between the models ~ 5 – 15 %.

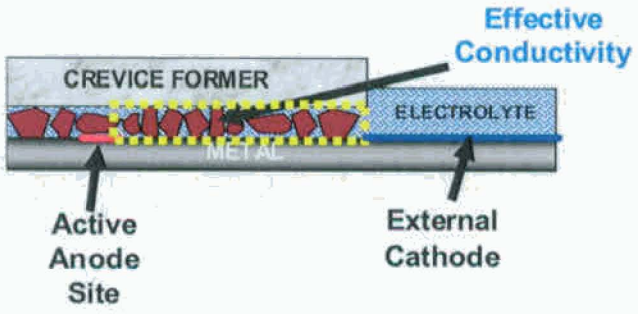

Figure 5: Schematic diagram depicting the presence of particulates under a crevice former.

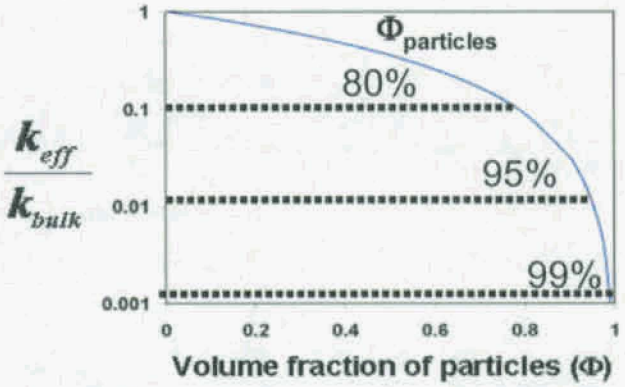

Figure 6: Effect of particle loading ($\phi_{particles}$) on the effective solution conductivity (κ_{eff}), according to Bruggeman's Equation.

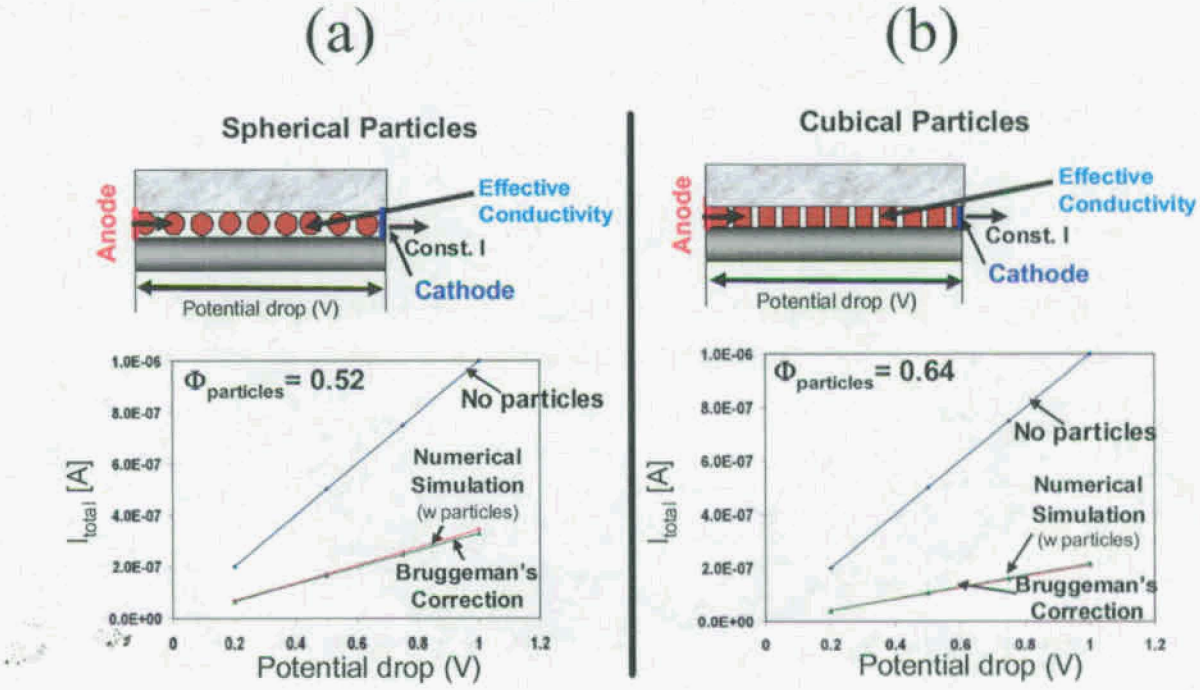

Figure 7: Comparison of the total current for a given potential drop for homogenous electrolyte (no particles) to numerical simulation in presence of particles, and to homogeneous electrolyte corrected for the volume effect using Bruggeman's equation. (a) Spherical particles; $\Phi_{particles}$ = 52%, (b) Cubical particles, $\Phi_{particles}$ = 64%.

Figure 8: SEM image of corrosion products observed in crevice corrosion tests for Alloy C-22 (8).

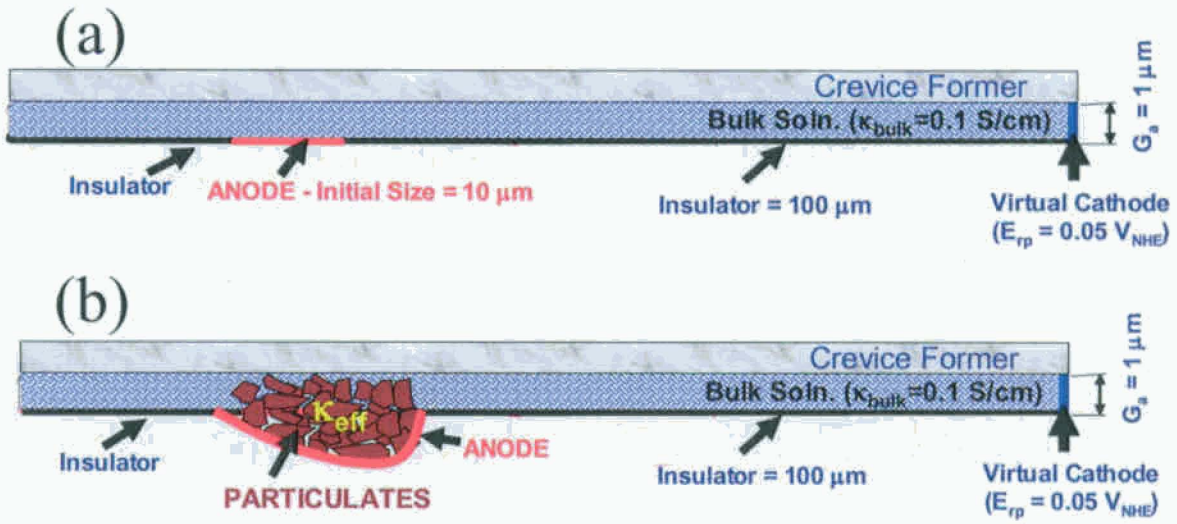

Figure 9: Schematic diagram of (a) the geometry used in simulating the effects of corrosion product accumulation on the crevice damage profile evolution, and (b) illustration of corrosion product accumulation at the corroding site.

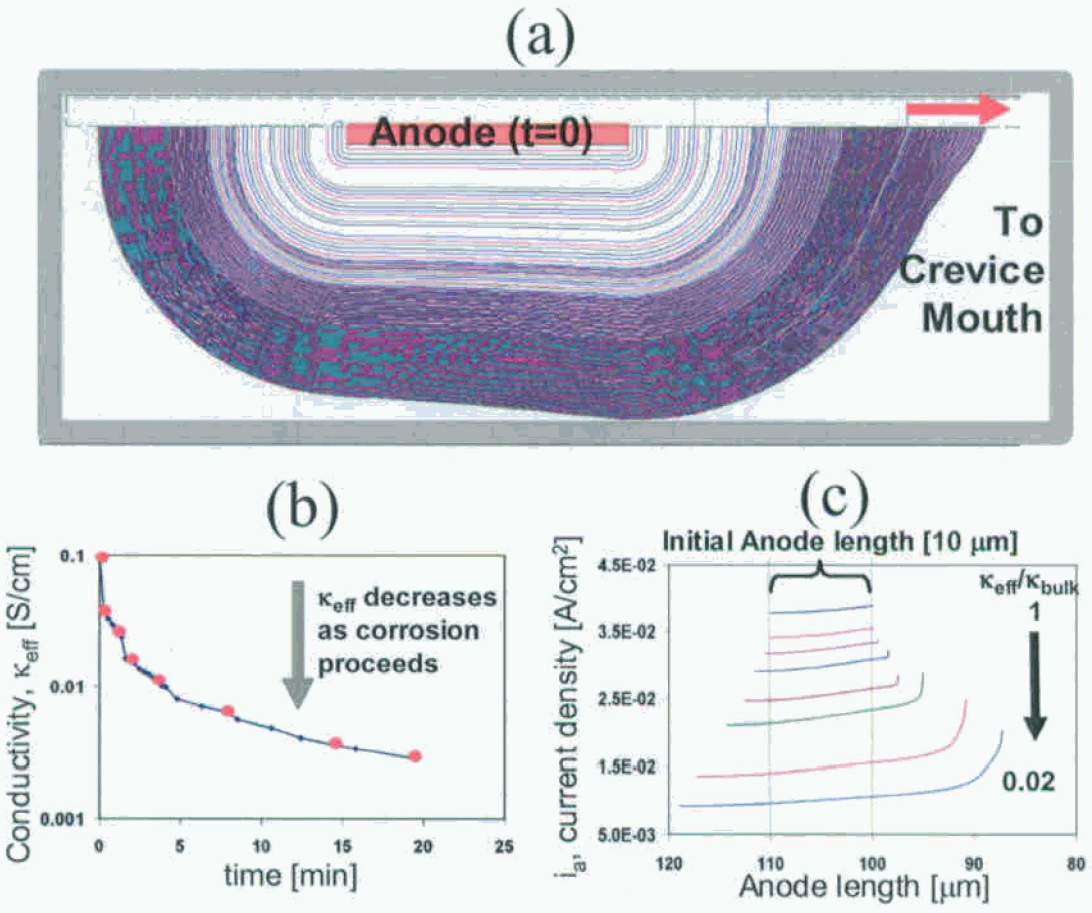

Figure 10: (a) Corrosion profile evolution in the presence of oxide accumulation. (b) Effective conductivity at a corrosion site corrected for the volume occupied by particles as a function of time. (c) Current density profile along the anode for different time steps corresponding to the increase in particulate volume.

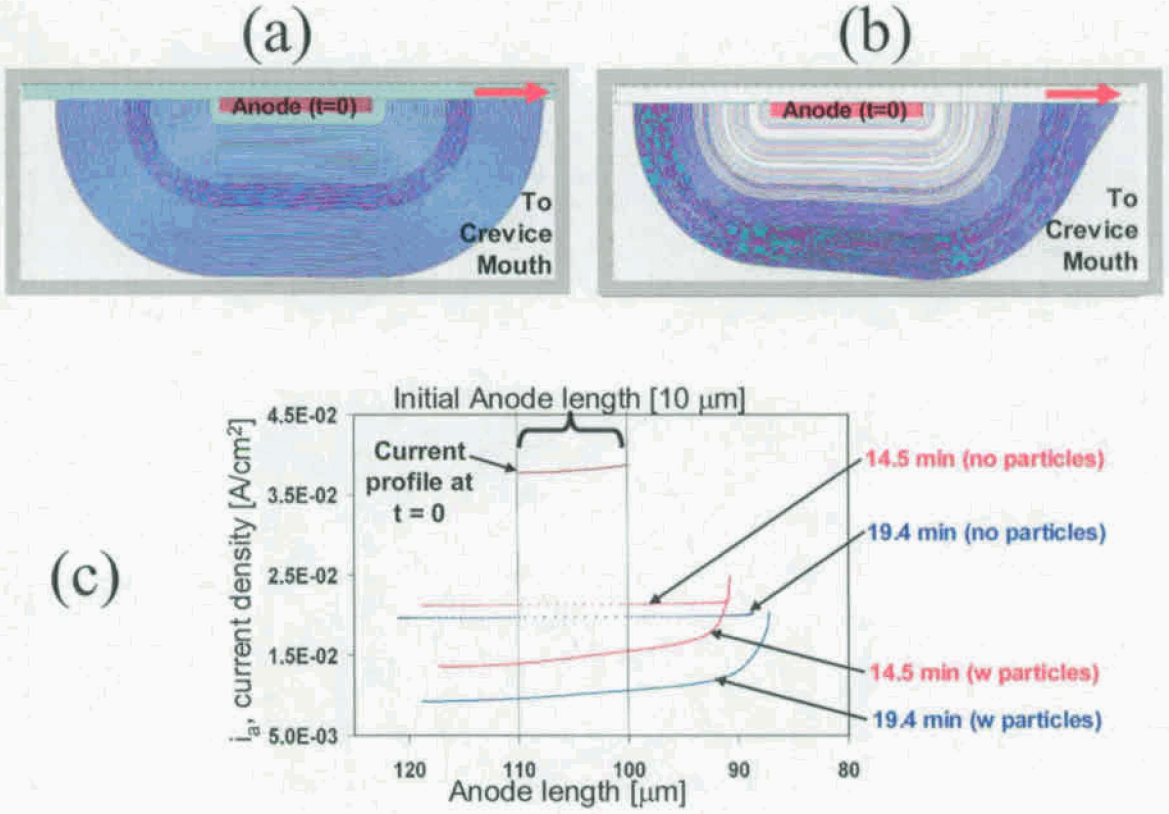

Figure 11: Comparison of the damage evolution profile with and without solid oxide accumulation at the corroding site. (a) Damage propagation without particulate accumulation at the corroding site [$\kappa = \kappa_{bulk}$ (constant)]. (b) Damage propagation in the presence of particulates [$\kappa_{eff} = \kappa_{bulk} \bullet (1-\Phi_{particles})^{3/2}$]. (c) Comparison of current density profiles on the anode with and without particle effects.